frontiers in Chemical Engineering

REVIEW
published: 22 March 2021
doi: 10.3389/fceng.2021.615309

Recent Advances in Photocatalytic Transformation of Carbohydrates Into Valuable Platform Chemicals

Huan Chen[1], Kun Wan[1], Fangjuan Zheng[1], Zhuo Zhang[1], Hongyu Zhang[1], Yayun Zhang[1] and Donghui Long[1,2]**

[1]State Key Laboratory of Chemical Engineering, East China University of Science and Technology, Shanghai, China, [2]Shanghai Key Laboratory of Multiphase Materials Chemical Engineering, East China University of Science and Technology, Shanghai, China

In response to the less accessible fossil resources and deteriorating environmental problems, catalytic conversion of the abundant and renewable lignocellulosic biomass to replace fossil resources for the production of value-added chemicals and fuels is of great importance. Depolymerization of carbohydrate and its derivatives can obtain a series of C_5-C_6 monosaccharides (e.g., glucose and xylose) and their derived platform compounds (e.g., HMF and furfural). Selective transformation of lignocellulose using sustainable solar energy *via* photocatalysis has attract broad interest from a growing scientific community. The unique photogenerated reactive species (e.g., h^+, e^-, $^{\bullet}OH$, $^{\bullet}O_2^-$, and $^1O_2$), novel reaction pathways as well as the mild reaction conditions make photocatalysis a "dream reaction." This review is aimed to provide an overview of the up-to-date contributions achieved in the selective photocatalytic transformation of carbohydrate and its derivatives. Photocatalytic methods, properties and merits of different catalytic systems are well summarized. We then put forward future perspective and challenges in this field.

Keywords: photocatalysis, lignocellulose, carbohydrates, platform chemicals, mechanisms

OPEN ACCESS

Edited by:
Qineng Xia,
Jiaxing University, China

Reviewed by:
Hu Li,
Guizhou University, China
Qineng Xia,
Jiaxing University, China

****Correspondence:***
Yayun Zhang
yy.zhang@ecust.edu.cn
Donghui Long
longdh@mail.ecust.edu.cn

Specialty section:
This article was submitted to Catalytic Engineering, a section of the journal Frontiers in Chemical Engineering

Received: *08 October 2020*
Accepted: *13 January 2021*
Published: *22 March 2021*

Citation:
Chen H, Wan K, Zheng F, Zhang Z, Zhang H, Zhang Y and Long D (2021) Recent Advances in Photocatalytic Transformation of Carbohydrates Into Valuable Platform Chemicals. Front. Chem. Eng. 3:615309. doi: 10.3389/fceng.2021.615309

INTRODUCTION

As a result of the increase in world population and rapid industrial development over the past century, the world has become increasingly dependent on nonrenewable fossil resources such as petroleum, coal to meet the growing demand and the increasingly challenging industrial and transportation technology requirements (Puga, 2016). Nowadays, about 85% of all fossil feedstocks consumed is used for the production of transportation fuels and only 10% for the production of chemicals (Climent et al., 2011). Against the backdrop of predicted depletion of worldwide mineral resources and growing concerns about political and environmental concerns such as global warming and deteriorating air quality, the focus of research is shifting to alternative and sustainable energy resources to produce inexpensive and transportable fuels that can be directly employed in current power generation systems (De et al., 2015; Hu et al., 2017). The production of carbon-neutral, low-emission biofuels and green chemicals from renewable resources, such as biomass, is particularly compelling in the progressive replacement of traditional fossils.

Biomass is the world's fourth largest energy source after oil, coal and natural gas (Li et al., 2015). Photosynthesis in nature produces 170 billion metric tons of biomass per year by fixing carbon from atmospheric CO_2. (Zhang and Wang, 2020). Plant material consisting mainly of carbohydrate polymers (cellulose and hemicellulose) and an aromatic polymer (lignin) is considered to be lignocellulose, which represents more than 90% of all plant biomass. The represented structure

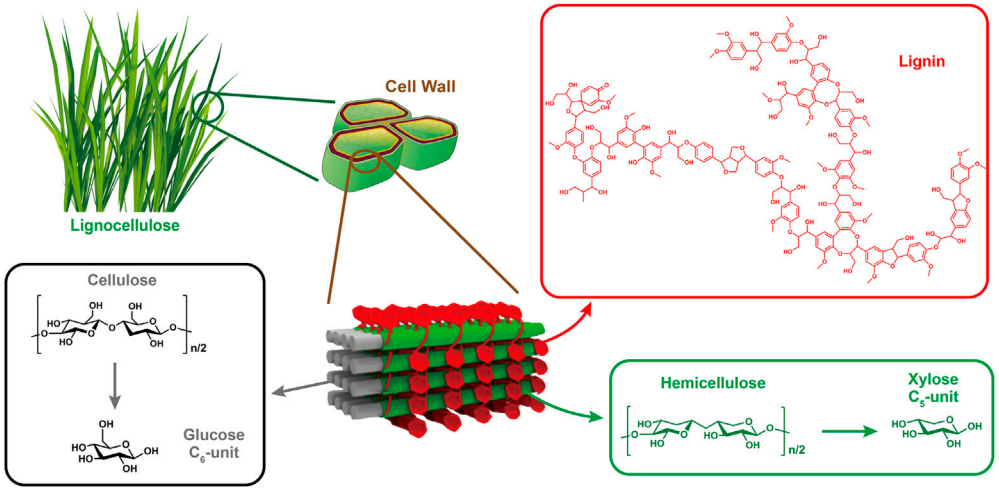

FIGURE 1 | Schematic of the structure of lignocellulose.

of lignocellulose is illustrated in **Figure 1**. Cellulose and hemicellulose are encapsulated in a lignin shelter. Cellulose fibers bind to hemicellulose and lignin by hydrogen bonding, while hemicellulose is covalently bound to lignin. The percentage of each component varies depending on the plant species, but generally, typical lignocellulose is composed of 35–50% cellulose, 25–35% hemicellulose, and 10–25% lignin (Wang and Wang, 2019). Carbohydrates, in particular, are promising as they are the largest source of natural renewable carbon by far (van Putten et al., 2013), and harbor great potential to produce a variety of value-added commodity chemicals (e.g., gluconic acid, 5-hydroxymethyl furfural (HMF), 2,5-furandicarboxylic acid (FDCA), levulinic acid (LA)) (Sheldon, 2014). Surprisingly, less than 5% of these biomass carbohydrates have so far been used by humans for a variety of purposes (Zhang et al., 2017b). A large portion of them is considered to be waste streams and remain underutilized at present. Their fate is burned to provide heat and energy for biorefinery and paper/pulp industries. It is worth noting that the use of vast amount of edible biomass as long-term feedstocks for the production of first-generation biofuels (biodiesel and bio-ethanol) require significant land input, thus posing a direct negative impact on global food supply. So recent researches have focused on the valorization of non-edible biomass or waste biomass generated during the production of edible crops (Sheldon, 2014). According to the International Energy Agency (IEA), biofuels could provide 10% of the world's primary energy supply by 2035, and replace 27% of the world's transportation fuel by 2050 (Wang et al., 2017). Thus, holistic utilization of the world's most abundant bio-resources could greatly alleviate energy crisis.

In traditional lignocellulosic biorefineries, thermochemical methods (i.e., pyrolysis, gasification and liquefaction) have been developed to transform carbohydrates into bio-oil, syngas or liquid fuels at high temperature and/or pressure, resulting in intensive thermal energy input. Biochemical treatment, including digestion and fermentation, is another useful method to convert biomass into biogas using costly peculiar enzymes, bacterial and microorganisms under anaerobic conditions. In contrast, Sun light as an inexhaustible energy source can be used to replace thermal energy. Photocatalysis, in which photons are used to drive redox reactions, represents a promising strategy to convert solar energy and renewable lignocellulose into valuable fuels and chemicals. The active photogenerated holes and electrons, as well as unique photo-induced reactive oxygen species (ROS) enable the precise cleavage of targeted chemical bonds. In addition, various functional groups can be retained under mild reaction conditions (Zhang, 2018).

A growing number of research articles dealing with photocatalytic conversion of carbohydrates (i.e., cellulose, glucose, HMF) into fuels and chemicals have been published. However, these contributions have not been comprehensively reviewed previously (Liu et al., 2019; Wu et al., 2020). In order to promote further development in such a promising area, there is a need for a timely and systematic review of up-to-date advances in this area. Therefore, this review is aimed to provide an overview of the state-of-the-art contributions achieved along the lines of selective photocatalytic transformation of carbohydrate and its derivatives. Future perspective and challenges in this field will also be emphasized. The authors hope that this review can provide guidance and inspiration to develop efficient photocatalyst for the valorization of carbohydrates.

PHOTOCATALYTIC TRANSFORMATION OF CELLULOSE

Cellulose represents the main component of the inedible lignocellulosic biomass on earth, along with hemicellulose and lignin. It is also the most important structural component in plants, providing strength and stability for plant cell walls and

fiber. Cellulose, with a general formula of $(C_6H_{12}O_5)_n$, possesses the simplest structure among other polysaccharides, as it is a homopolymer composed of glucose in the form of β-D-anhydroglucopyranose units (AGUs) that covalently linked to each other by β-1,4-glycosidic bonds between the equatorial OH groups of C_4 and the C_1 carbon atoms (Credou and Berthelot, 2014). The number of repeating AGUs constituting the polymer chain is defined as the degree of polymerization (DP) of cellulose. For instance, the common DP value of cellulose derived from wood pulp is around 300–1700, whereas the value is about 800–10,000 in cotton or other plant fibers (Klemm et al., 2005). Large number of hydroxyl groups along the skeleton form intra- and inter-molecular hydrogen bonds with oxygen atoms on the same or another chain, holding the chains firmly to form microfibrils with high tensile strength. Thus, dissolution of cellulose without chemical modification in common solvents is rather difficult to achieve (Hu et al., 2015; Shaghaleh et al., 2018). It was reported that this hydrogen-bonding network could be broken with concentrated $ZnCl_2$ owing to the interaction between ionic species and hydroxyl groups (Fan et al., 2011).

The selective transformation of cellulose into various high-value bio-based chemicals and high-quality fuels has drawn intensive attention in the field of biorefinery. It should be pointed out that hydrolytic cleavage of the β-1,4-glycosidic bonds between two anhydroglucose units to produce glucose is the starting point for other catalytic transformations (Huang and Fu, 2013). Owing to its crystalline structure and the robust intra- and intermolecular hydrogen bonding interaction, hydrolysis of cellulose is significantly challenging. More recently, it was found that localized surface plasmon resonance (LSPR) effect has a potential in facilitate biomass conversion. Compared with traditional heating method, LSPR-induced photothermal heating is more effective and straightforward toward intended reaction sites. It was first reported that TiO_2 nanofibres supported H-form Y-zeolites (HY) decorated with Au nanoparticles (denoted as Au-HYT) showed an enhanced ability in cellulose hydrolysis under visible light irradiation (Wang et al., 2015). Pores on nanozeolites were elaborately controlled to facilitate mass transfer of dissolved cellulose into the porous channel to interact with the active site. The decorated plasmonic Au NPs absorb visible light and enhance the polarized electric field of zeolites, which also contributes to the increase in acid strength. Both glucose and HMF were detected as main hydrolysis products, with a total yield of more than 60% at 130°C for 24 h. The yield of glucose increased with an increase in light intensity, indicating that the conversion of cellulose is truly enhanced by LSPR effect.

Also based on the LSPR effect, Ir/HY zeolite catalyst exhibited a different mechanism for the hydrolysis of cellobiose, a dimer of glucose with β-1,4-glycosidic bonds (Zhang et al., 2018a). The role of Ir NPs and HY zeolite were carefully clarified. Under visible light irradiation, the highest temperature of Ir/HY reached 106°C, while the temperature of HY zeolite without Ir NPs was only about 40°C. This result demonstrated that the plasmonic photothermal effect of Ir NPs effectively converts light into thermal energy, increasing the local temperature of the surface of Ir/HY catalysts, thus accelerating the catalytic hydrolysis of cellobiose. Meanwhile, the acidic sites of HY zeolite as active centers are responsible for the hydrolysis of cellobiose. The role of the acid strength of the solid acid catalysts in activating crystalline cellulose toward hydrolysis was further explored. Generally, HY zeolites with higher ratios of Si/Al have stronger acidity. The observed activity is in the order of Ir/HY_3 (Si/Al = 11)> Ir/HY (Si/Al = 7)> Ir/HY_2 (Si/Al = 5.2), suggesting that the acid density of the solid acid catalyst is directly correlated with catalytic activity. Only glucose and HMF were detected, which were derived from the breakage of β-1,4-glycosidic bonds, not from the C–C bonds cleavage, indicating very high selectivity (>99%). This is in accordance with the results reported by Wang (Wang et al., 2015). Ir/HY_3 and Ir/Amberlyst-15 resin (a strong commercial protonic solid acid) catalysts were further applied to treat non-pretreated crystalline cellulose. Under visible light irradiation, the yield of atotal products was up to 75.3% at 90°C and 72.6% at 70°C, respectively.

Although great progresses have been made in photo-enhanced solid acid-catalyzed hydrolysis of cellulose, mass diffusion between crystalline cellulose and solid acid catalyst still impedes the efficient cellulose transformation. Concurrent modification of TiO_2 photocatalyst with chemisorbed sulfate (SO_4^{2-}) and nickel sulfide (Ni_xS_y) endows TiO_2 with another identity as a solid acid catalyst (Hao et al., 2018). The SO_4^{2-} species bound to the TiO_2 surface by coordination facilitate cellulose hydrolysis into glucose which is more attainable to catalyst (**Figure 2**). Photogenerated holes oxidize the water to generate $^{\bullet}OH$ radicals, which attack glucose to produce protons and formic intermediate. Meanwhile, Ni_xS_y cocatalyst favors charge separation and act as hydrogen evolution sites for H_2 generation. However, the accumulated formate may adsorb on the catalyst surface and occupy the corresponding active sites to decrease the H_2 evolution rates. A significant elevation in H_2 yield was achieved using TiO_2-SO_4^{2-}-Ni_xS_y, reaching 3.02 mmol $g^{-1}h^{-1}$ on average during the first 3 h, which was approximately 76 times higher than that of pristine P25.

Zhang et al. developed a photocatalytic system for the photo-reforming cellulose into H_2 in neutral aqueous solution by loading a graphitic carbon layer on TiO_2/NiO_x nanoparticles (denoted as $TiO_2/NiO_x@C_g$) (Zhang et al., 2018b). Enhanced H_2 production yields of ~270 μmol h^{-1} g^{-1} and ~4,000 μmol h^{-1} g^{-1} were obtained at room temperature and 80°C, respectively. The significant enhancement of the hydrogen production rate may be because the higher temperature promotes the dissolution of a portion of suspended carbohydrate fragments, which provides solvated cellulose as substrate for photocatalysis. The mechanism of the process has been proposed in **Figure 3**. Upon light irradiation, the deposited NiO_x is reduced to metallic Ni by the photogenerated electrons from TiO_2. A proton is withdrawn from the –OH group of the alcohol adsorbed on the Ni surface and subsequently reduced by the electron to obtain a Ni-H hydride. The presence of the carbon layer weakens the interaction of H with the Ni metal surface, generating a molecule of H_2. Meanwhile, alkoxide anion left behind is oxidized to CO_2, CO, CH_4 by holes.

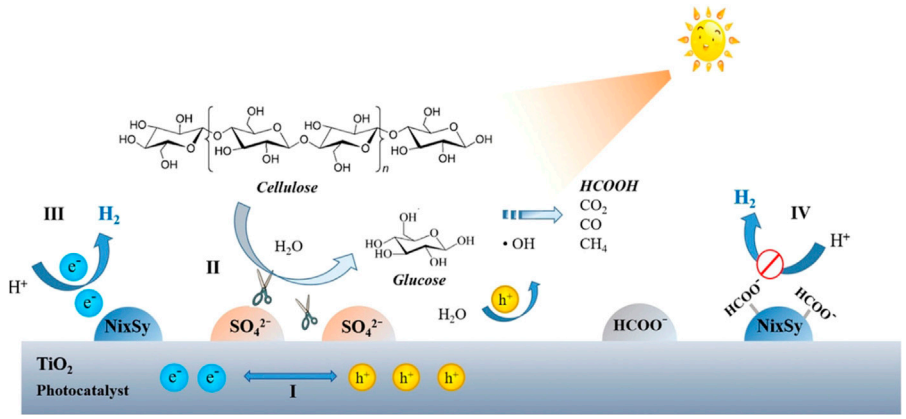

FIGURE 2 | Proposed mechanism of photo-reformation of cellulose into H_2 using TiO_2-SO_4^{2-}-Ni_xS_y.

PHOTOCATALYTIC OXIDATION OF GLUCOSE

Glucose is the most abundant and cheapest monosaccharide in nature, which can be easily obtained by hydrolysis of polysaccharides such as cellulose and starch (Deng et al., 2014; Chatterjee et al., 2015). With six carbon atoms, glucose is classified as hexose and it can exist in an open-chain form as well as a cyclic form. In its open-chain form, the glucose molecule has an open and unbranched six-carbon backbone, where C_1 is part of an aldehyde group and each of the other five carbons bears a hydroxyl group. Therefore, glucose is also known as aldose or aldohexose. The aldehyde group makes glucose a reducing sugar giving a positive result with the Fehling solution. The cyclic form is the result of an intramolecular reaction between the aldehyde C_1 atom and the C_5 hydroxyl group to form an intramolecular hemiacetal.

Selective oxidation of glucose can produce a wide range of value-added chemicals, such as gluconic acid, glucaric acid, formic acid and so on (**Figure 4**). These products as valuable platform chemicals have been widely used in many fields. For example, gluconic acid is widely used as food additive, concrete ingredient medical intermediate and precursor for biodegradable polymers (Climent et al., 2011). Glucaric acid, regarded as one of the top value-added chemicals from biomass, is a key building block for producing various functional polymers including new nylons and hyperbranched polyesters (Kiely et al., 1994). Formic acid as an important intermediate is widely used in chemical synthesis and also has the potential to serve as an excellent hydrogen carrier because the dehydrogenation of formic acid can easily proceed under mild conditions using catalysts (Guerriero et al., 2014).

Traditional oxidation of glucose has been extensively studied through fermentation and erobic catalytic oxidation (Benkó et al., 2014; Haynes et al., 2017; Liu et al., 2017). However, the fermentation process proceeds relatively slow, which is greatly depend on the enzyme activity. Aerobic oxidation using heterogeneous catalysts based on precious metal nanoparticles (i.e., Au, Ag, Pd, and Pt) was usually carried out at high temperature and pressure, resulting in a low performance-price ratio and security risks. In contrast to these energy intensive processes, recent application of heterogeneous photocatalysts in the transformation of glucose with oxygen as the terminal oxidant has received increasing attention because photocatalytic transformation is driven by solar energy and can be conducted at room temperature and atmospheric pressure. TiO_2-based photocatalysts are the most widely used owing to their non-toxicity, low cost and excellent stability. A powdered TiO_2 photocatalyst was synthesized by an ultrasound-promoted sol-gel method for the selective photo-oxidation of glucose to glucaric acid, gluconic acid and arabitol. Experiment results indicated that a mixture of 50:50 H_2O: ACN (v/v) was the best solvent composition. After 10 min of irradiation, glucose conversion reached 11% and total organic selectivity was up to 71.3%. The relatively high carboxylic acids selectivity could be attributed to lower affinity of these acids on TiO_2 (US) surface in the presence of acetonitrile as "stabilizing agent". Meanwhile, lower amount of water might give rise to a lower concentration of nonselective $^{\bullet}OH$ radicals (Colmenares et al., 2011).

A more selective zeolite Y-supported TiO_2 photocatalyst was fabricated, offering total selectivity of gluconic and glucaric acid

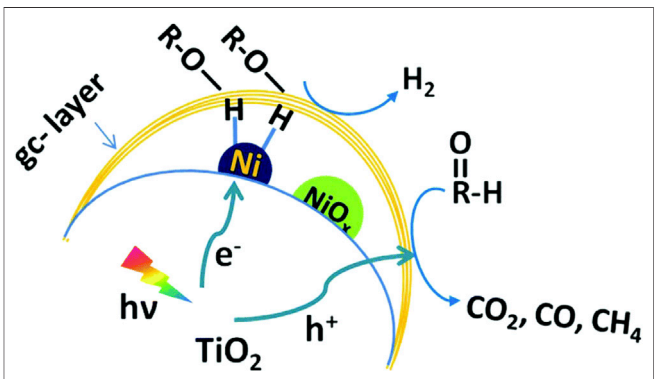

FIGURE 3 | Proposed potential mechanism of the photoreforming of cellulose by $TiO_2/NiO_x@C_g$.

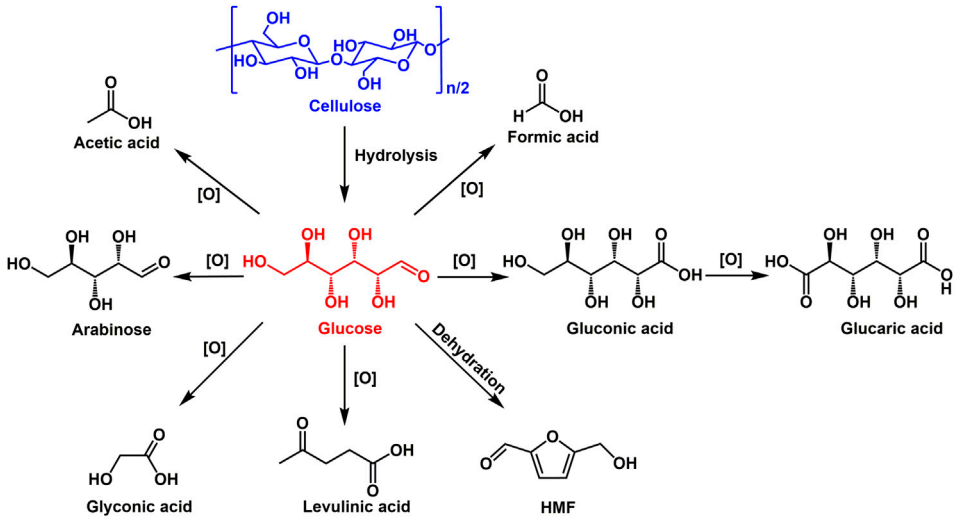

FIGURE 4 | Chemicals produced by oxidation of glucose.

up to 68%. The electrostatic repulsion between negatively charged zeolite framework and carboxylic acids facilitated the desorption of organic acids, preventing subsequent mineralization (Colmenares and Magdziarz, 2013). This kind of electrostatic repulsion also exists in the alkaline suspension of nano-TiO_2. A formate yield of 35% and high conversion of glucose up to 100% at ambient condition with 0.03 M NaOH was achieved. The precise control of the amount NaOH is fundamental in the conversion of glucose because appropriate amount of hydroxyl ions can not only promote the formation of active oxidative radicals ($^{\bullet}O_2^-$, $^{\bullet}OH$), but also make the surface of TiO_2 negatively charged. The repulsive forces between formate ions (HCO_2^-) and TiO_2 surface would facilitate the desorption of formic acid and then a high formate selectivity can be obtained (Jin et al., 2017).

The incorporation of Cr^{3+} or Fe^{3+} ions into TiO_2 lattice would slightly reduce the bandgap to the value of 3.04 or 2.3 eV, compared with generally accepted 3.2 eV for anatase TiO_2. A total organic acid selectivity of 87% at a 7% glucose conversion was obtained for Cr-doped TiO_2/zeolite, and the Fe-modified TiO_2/zeolite offered a 94.3% selectivity to glucaric and gluconic acid (Colmenares et al., 2013a; Colmenares et al., 2013b). The effect of co-doping on the physicochemical properties of TiO_2 for the conversion of glucose into value-added chemicals were rarely reported. When TiO_2 is co-doped by boron (B) and nitrogen (N), the introduction of foreign B and N element results in the formation of localized states near the CB and VB in the bandgap of TiO_2, respectively. Excitations from these localized states to the CB of TiO_2 may be responsible for the red shift of the absorption edge toward the visible region. For Ag/N-doped TiO_2 catalyst, Ag acts as electron traps to facilitate charge separation. The improved charge separation and increased active surface area lead to enhanced generation of hydroxyl radicals, which further oxidize glucose to various high-value chemicals (Suriyachai et al., 2020).

In evaluating the performance of a photocatalyst, we typically focus on the ease of electron-hole pair separation, charge mobility and the rate at which the active species is produced. However, the interaction between substrate and photocatalyst surface is sometimes overlooked, but this is exactly what is crucial and may provide new understanding of the reaction pattern. Visible-light selective photocatalytic conversion of glucose using unmodified TiO_2 is achieved through the formation of a glucose-TiO_2 charge transfer complex (Da Vià et al., 2017). The formation of this kind metal-organic complex responds for the visible-light absorption ability of the TiO_2 and allows the direct transfer of photo-excited electrons from the highest occupied molecular orbital of glucose to the conduction band of the TiO_2 (Kim et al., 2015). Optimization of the reaction conditions resulted in 42% glucose conversion under visible light with 7% selectivity to gluconic acid and 93% selectivity to other partial oxidation products.

Han et al. reported that TiO_2 supported Au nanoparticles was very efficient and selective in glucose oxidation under both UV and visible light in Na_2CO_3 aqueous solution (Zhou et al., 2017).

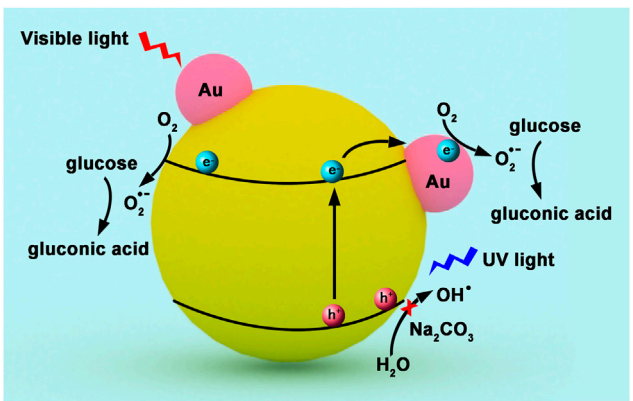

FIGURE 5 | Proposed mechanism for **(A)** visible light, and **(B)** UV light-induced glucose oxidation by Au/TiO_2 in aqueous Na_2CO_3 solution.

Both glucose conversion and gluconic acid yield were up to 99% under visible light irradiation for 4 h. It is interesting that the electron generation and transfer in Au NPs/TiO_2 is completely different under visible and UV light irradiation (**Figure 5**). Under visible light, electrons induced by LSPR effect were released from Au NPs and injected into the conduction band of TiO_2. Then, these photoactivated electrons activated O_2 to form active superoxide radical ($^{\bullet}O_2^-$), which further participated in the oxidation of glucose. When Au NPs/TiO_2 was irradiated by UV light, photogenerated holes were excited to the conduction band of TiO_2 from the valence band. Au NPs trapped the electrons and served as reaction sites for the generation of $^{\bullet}O_2^-$, which oxidized the glucose into gluconic acid. Meanwhile, Reactive oxygen species (e.g., $^{\bullet}OH$ and $^1O_2$) with strong oxidization power were inhibited by Na_2CO_3, leading to a high selectivity of desired product.

Inspired by natural enzymes that exhibit both high activity and selectivity in bioreactions, a strategy of mimicking enzyme center to prepare novel biomimetic catalyst for selective oxidation reactions has been developed. Metallothioporphyrazines (MPz), a sulfur-containing macrocyclic compound with extensive conjugated system of delocalized π-electrons and strong visible light absorption ability, has been considered as one of the most promising biomimetic photocatalysts (Zhou et al., 2016; Li et al., 2018). Under visible light irradiation, MPzs can activate hydrogen peroxide or oxygen for the selective organic transformation and pollutant degradation. Several kinds of metallothioporphyrazines with different supports were prepared and further applied to the photocatalytic oxidation of glucose, such as H-ZSM-5-supported FePz $(SBu)_8$ (Chen et al., 2019), SnO_2-supported FePz $(SBu)_8$ (Zhang et al., 2019), TiO_2/HPW/CoPz (Yin et al., 2020), and ZnO-supported $CoPzS_8$ (Cheng et al., 2019). For example, a TiO_2/HPW/CoPz biomimetic photocatalyst was synthesized by modifying TiO_2 with HPW and CoPz (Yin et al., 2020). Glucose was oxidized into gluconic acid and glucaric acid with molecular oxygen in only water without the addition of H_2O_2. Under optimized conditions, total selectivity for both acids reached up to 80.4% at a 22.2% glucose conversion. It is interesting that HPW and CoPz had synergistic effect on glucose oxidation. On one hand, the presence of CoPz not only improved the separation of photogenerated charges and accelerated the formation of active species but also increased the adsorption capacity of glucose on catalyst surface, resulting in a higher glucose conversion. On the other hand, the introduction of HPW increased the surface acidity of the catalyst. The repulsive force facilitates the desorption of carboxylic acids (glucaric and gluconic acids) from the catalyst surface. Therefore, further oxidation was inhibited and a higher selectivity to both acids was obtained.

PHOTOCATALYTIC TRANSFORMATION OF HMF AND FURFURAL

5-hydroxymethylfurfural (HMF) and furfural, the dehydration product of C_5 and C_6 carbohydrates, are deemed as versatile intermediates in biomass conversion and key platform compounds for the production of value-added industrial and pharmaceutical chemicals. (Zakrzewska et al., 2011; Hu et al., 2017). The marvelous and reactive structure containing an furan ring and an aldehyde group allow HMF to undergo a variety of reactions, such as oxidation, hydrogenation, etherification et al., to produce high-quality biofuels such as 2,5-dimethylfuran (DMF), 2,5-dimethyltetrahydrofuran (DMTHF), 5-ethoxymethylfurfural (EMF) and new-fashioned high-value chemicals such as levulinic acid (LA), 2,5-diformylfuran (DFF), 2,5-dihydroxymethylfuran (DHMF) and 2,5-furandicarboxylic acid (FDCA) (**Figure 6**) (Hu et al., 2018). Among them, much attention has been paid to DFF and FDCA. DFF can be widely used in the production of furan-based polymers, organic conductors, and intermediates of pharmaceuticals and antifungal agents. FDCA was regarded as one of the top 12 value-added chemicals from biomass by the United States Department of Energy in 2004, and has been deemed as an important building block for the production of biochemicals and has the potential to be a renewable alternative to terephthalic acid to produce polyethylene terephthalate (PET) plastics (Zhang and Deng, 2015).

Given that much more interest and attention have been paid to the furan-based derivatives, the state-of-the-art advances on the photocatalytic transformation of furan-based derivatives *via* oxidative and reductive approaches are systematically summarized and discussed (**Table 3**).

Photo-Oxidation Reactions

Since the pentatomic furan ring is not as stable as that of the hexatomic aromatic structures, it is not surprising that overoxidation and/or mineralization often occurs in HMF transformation when strong oxidizing species are generated in the photocatalytic system, resulting in poor product selectivity. In 2013, HMF was reported to be photocatalytic oxidized to DFF with home-prepared TiO_2 for the first time (Yurdakal et al., 2013). TiO_2 nanoparticles with three different crystalline phases (anatase, rutile, and brookite) were prepared *via* a sol-gel method, but their crystallinity was far less than commercial TiO_2 catalyst. A DFF selectivity of 22% was obtained under ultraviolet (UV) irradiation. The low selectivity might be ascribed to the generation of highly oxidized $^{\bullet}OH$ radicals, which unselectively attack the furan ring of HMF and mineralize them into CO_2 and H_2O. Nitrogen doping can boost DFF selectivity to 30–40% (Krivtsov et al., 2017b). It was proposed that the N-species on the TiO_2 modified its surface chemistry by reducing the hydroxylation degree. Thus, the transfer of unselective $^{\bullet}OH$ radicals from TiO_2 surface to products can be suppressed.

In comparison, g-C_3N_4 possesses a moderate band gap of around 2.7 eV. The less positive VB edge make g-C_3N_4 hard to oxidize water or OH^- to produce unselective $^{\bullet}OH$ radical by photogenerated holes. However, the more negative CB potential is in favor of activating O_2 to generate superoxide radical ion ($^{\bullet}O_2^-$), which is a key oxidative species for HMF oxidation. Metal-free g-C_3N_4 was synthesized by a simple calcination of melamine. The addition of water favored the formation of pore

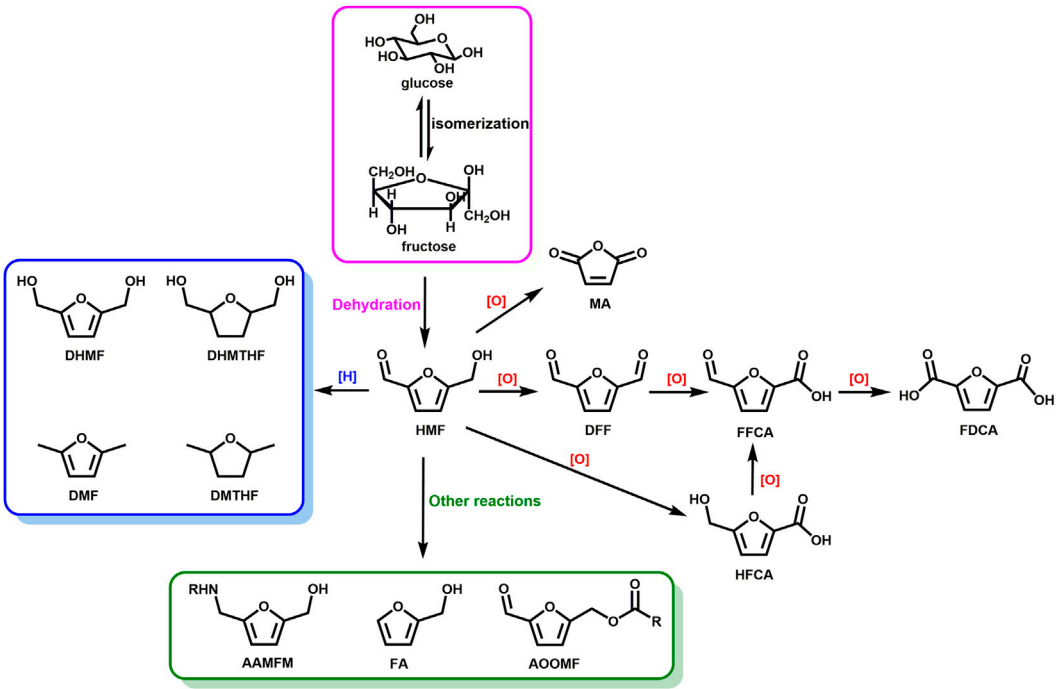

FIGURE 6 | Catalytic conversion of HMF into various valuable products. DFF, HFCA, FFCA, MA, FDCA, DHMF, DHMTHF, DMF, DMTHF, AAMFM, FA, and AOOMF denote 2,5-diformylfuran, 5-hydroxymethyl-2-furancarboxylic acid, 5-formyl-2-furancarboxylic acid, maleic anhydride, 2,5-furandicarboxylic acid, 2,5-dihydroxymethylfuran, 2,5-dihydroxymethyltetrahydrofuran, 2,5-dimethylfuran, 2,5-dimethyltetrahydrofuran, 5-arylaminomethyl-2-furanmethanol, furfuryl alcohol, and 5-alkanoyloxymethylfurfural.

structure and enhanced specific surface area and pore volume. It was found that O_2 is indispensable in HMF oxidation, since it is the source of $^{\bullet}O_2^-$ radical, which is determined as the dominant active species. The addition of polar solvents decreased the HMF conversion, probably because they prone to compete with the HMF for the active sites. Benzotrifluoride ($PhCF_3$) was found to be the best solvent due to its less polarity and superior ability for O_2 dissolvent (Wu et al., 2017).

A bulk g-C_3N_4 catalyst was prepared *via* the thermal condensation method from different precursors (melamine, urea and thiourea). Only a 28% selectivity of DFF was obtained under solar light irradiation for 4 h. The thermal exfoliation procedure applied to bulk g-C_3N_4 increased the selectivity to 42%, which can be attributed to the increased specific surface area of thermally exfoliated g-C_3N_4 nanosheets (Krivtsov et al., 2017a). The addition of *p*-benzoquinone significantly inhibited the reaction, indicating that $^{\bullet}O_2^-$ radicals were mainly responsible for the HMF oxidation. Changing the reaction atmosphere to nitrogen did not completely terminate the reaction, but almost no DFF was detected (Krivtsov et al., 2017a), probably due to the interaction of HMF with the surface functional groups (e.g., amino groups) of g-C_3N_4 (Ilkaeva et al., 2018). The formation of hydrogen bond between $-NH_2$ groups and water allows it been attacked by the photogenerated holes to form localized $^{\bullet}OH$ radicals (**Figure 7A**). The reaction of HMF with $^{\bullet}OH$ radicals leads to the ring opening and the formation of aliphatic intermediates, thus reducing the selectivity of DFF (**Figure 7B**). However, after the reaction of g-C_3N_4 with H_2O_2 to give g-C_3N_4-H_2O_2 adduct, H_2O_2 blocks the amino-groups of the g-C_3N_4, thus creating a steric hindrance for the HMF molecule interaction with the g-C_3N_4 surface sites (**Figure 7C**). The conversion of HMF may decreased slightly due to the absence of $^{\bullet}OH$ radicals, but the selectivity of DFF increased to 88% in return (Ilkaeva et al., 2018).

Photocatalytic oxidation of HMF to FDCA has been reported by immobilizing biomimetic cobalt thioporphyrazine (CoPz) on g-C_3N_4 (CoPz/g-C_3N_4) (Xu et al., 2017). CoPz molecules are hydrophobic and prone to aggregate in aqueous solutions, thus reducing the contact between the CoPz catalyst and substrates and finally giving a modest 40.2% HMF conversion and 36.2% FDCA yield. However, the hydrophilicity of g-C_3N_4 reduces the aggregation of the CoPz/g-C_3N_4 in the aqueous solution, making the catalytic active sites of CoPz more accessible to HMF. Excellent HMF conversion (99.1%) and selectivity to FDCA (96.1%) was achieved under the same conditions. Photocatalytic oxidation of HMF to FDCA just requires moderately active species such as $^1O_2$, while HMF can be completely mineralized to CO_2 by $^{\bullet}OH$ radical due to its high oxidizing potential. EPR results and control experiment indicated that $^1O_2$ is the dominant oxidative species for the HMF oxidation to FDCA. The synergistic interaction between CoPz and g-C_3N_4 not only promoted $^1O_2$ generation ability of CoPz under light irradiation but also inhibit the generation of $^{\bullet}OH$ radical. The

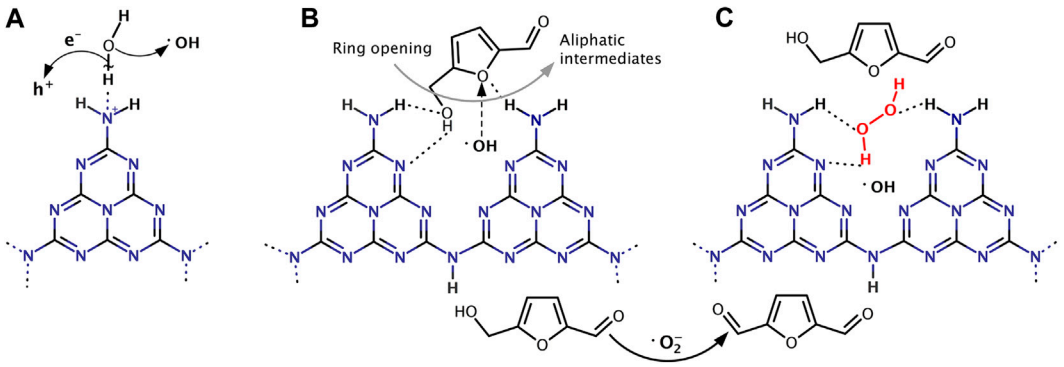

FIGURE 7 | (A) Hypothetical mechanism of hydroxyl radical formation on g-C_3N_4 basic sites. **(B)** Proposed types of interaction and photooxidation of HMF on g-C_3N_4, and **(C)** on g-C_3N_4-H_2O_2.

light excitation of pyrrole rings in CoPz molecule results in excited CoPz* with higher electronic cloud density. CoPz* exhibits much higher photocatalytic activity and activates O_2 to $^1O_2$ species, which possess suitable oxidation power to selectively oxidize HMF to the desired product FDCA. Then the excited CoPz* come back to its ground state (**Figure 8D**). In addition, pH value of the reaction system was found to be a crucial factor in product selectivity. At pH = 6.86 or 9.18 HMF was selectively oxidized to FDCA with a high selectivity above 97%. While at low pH (4.01), the selectivity of FDCA was less than 10% (**Figures 8A–C**).

Analogous control of product selectivity by adjusting pH was also reported by Sun et al. (Han et al., 2017). The authors found that nearly complete photocatalytic oxidation of HMF to DFF was realized by ultrathin CdS nanosheets loaded with cocatalyst Ni (Ni/CdS) under strong alkaline conditions (**Figure 8E**). This can be attributed to the Cannizzaro mechanism that aldehyde groups are not stable at high pH and will disproportionate to form alcohols and acids. An interesting phenomenon was also observed that almost 100% of furfural alcohol was oxidized to furfural after 22 h photocatalysis, while only 20% HMF conversion was achieved under the same condition (**Figure 8F**). DFT calculations and control experiments with DHMF and HMFCA as substrates indicated that HMF prefers to adsorb at water/NiO (001) interface *via* the −CHO group, impeding the oxidation of −OH group attached to the furan ring (**Figure 8G**). However, the presence of ancillary −OH and −COOH group did not present any negative impact. Photoluminescence and ^{1}H NMR results demonstrated that nearly no $^{\bullet}$OH radicals were generated during the photocatalysis process, which is consistent with Xu's results (Xu et al., 2017). Moreover, the photocatalytic activity could be enhanced by introducing nitrate salts (e.g., lithium, magnesium, calcium, and manganese) as redox mediator (DiMeglio et al., 2019).

In recent studies, HMF was often used as a sacrificial agent in the photocatalytic H_2 evolution by water splitting. Replacing water with D_2O, the detected D_2 indicated that the majority of H_2 is generated by the reduction water. The addition of co-catalyst Pt on the porous carbon nitride has no significant effect in the oxidation of HMF to DFF, but only contributes to the charge separation and form Pt-H bonds to reduce protons to H_2 (Battula et al., 2019). However, with NiS as cocatalyst, a Schottky barrier is formed at the interface between NiS and $Zn_3In_2S_6$, leading to the spatial separation of photoexcited charges (Meng et al., 2020). The H_2 evolution rate and DFF production in HMF solution reached up to 120 and 129 μmol $h^{-1}g^{-1}$, which are 41.4 and 35.8 times higher than that of pure $Zn_3In_2S_6$. In this work, the author confirmed the thermodynamics feasibility of the photocatalytic HMF-to-DFF oxidation and H_2 generation process. The VB potential of $Zn_3In_2S_6$ is 1.83 eV, which stands between the $E_{HMF/DFF}$ (1.61 eV) and $E_{DFF/oxidized\ DFF}$ (2.03 eV). This means the photogenerated holes generated on the valence band of $Zn_3In_2S_6$ can directly oxidize HMF to produce DFF, but cannot further oxidize DFF. On the other hand, the CB potential of $Zn_3In_2S_6$ (−0.97 eV) is more negative than the reductive potential of H_2 evolution (0 V). The HMF molecular is firstly deprotonated to form an alkoxide, which further react with a photoexcited hole to generate a carbon radical. The formed carbon radical is oxidized by a hole to produce a DFF molecular. Simultaneously, two protons, abstracted from HMF, are reduced by two electrons o produce a H_2 molecular.

The photocatalytic oxidation of HMF to DFF with Nb_2O_5 under visible light was reported by Wu's group (Zhang et al., 2017a). A high DFF selectivity (90.6%) from HMF was observed using Nb_2O_5 in benzotrifluoride in the presence of O_2 under visible light irradiation, although the bandgap energy of Nb_2O_5 is >3.2 eV. They determined that the alcoholic hydroxyl group of HMF can be adsorbed on Nb_2O_5 to form alcoholate species, decreasing the bandgap energy of Nb_2O_5 to the visible range. However, the DFF yield was not very satisfactory (<20%). Compared with Nb_2O_5-300 and Nb_2O_5-500, Nb_2O_5 treated at 800°C exhibits better photocatalytic activity, which is attributed to its high crystallinity, delaying the recombination of photogenerated charge carriers. MnO_2 nanorods could also catalyze a nearly complete conversion HMF to DFF (99% conversion, ~100% selectivity) without any additives (bases or oxidants). The oxidation was realized through a redox cycle between Mn^{4+} and Mn^{3+} (Giannakoudakis et al., 2019). The detection of trace amount of Mn_2O_3 phase on the spent catalyst

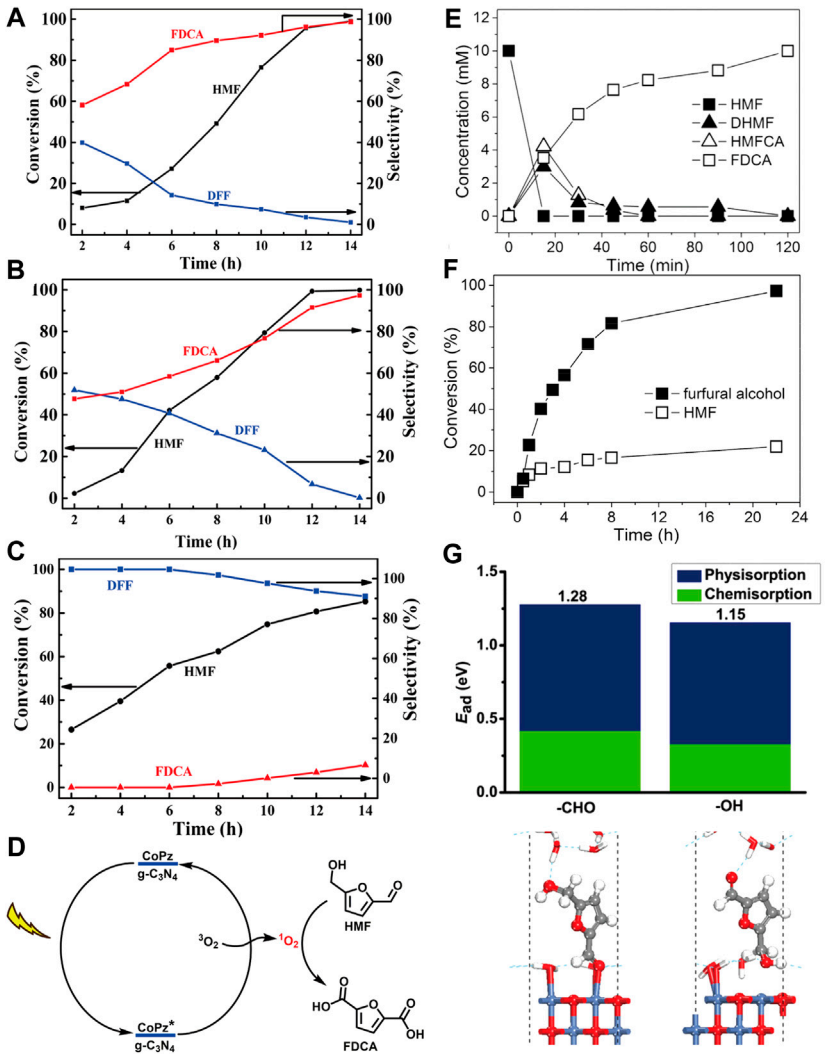

FIGURE 8 | Influence of pH of the reaction mixture on the photocatalytic performance: **(A)** pH = 9.18; **(B)** pH = 6.86; **(C)** pH = 4.01. **(D)** Possible mechanism of the photocatalytic Oxidation of HMF into FDCA with the CoPz/g-C_3N_4. **(E)** Concentration profile of HMF and its oxidation products (alkaline condition) over time. **(F)** Comparison of conversion of furfural alcohol and HMF in neutral water. **(G)** Adsorption structures and energies of HMF at water/NiO (001) interface *via* its aldehyde group or alcohol group.

by XRD confirmed the formation of Mn^{3+} intermediate state. Light irradiation promoted the activation of lattice oxygens on the nanorods and then facilitated the adsorption of HMF *via* the −C−OH on the O^- sites (**Figure 9**). However, the generated water molecules may form hydrogen bonds with the hydroxyl groups of HMF to inhibit its direct interaction with catalytic surface centers, resulting in a decreased conversion as reaction proceeded. The use of aprotic and less polar solvent will have a positive impact.

Most previous studies of HMF oxidation were carried out using noble metals in alkaline aqueous solutions at high O_2 pressure and elevated temperature. Another innovative approach to achieve HMF oxidation is electrochemical oxidation, where the oxidation capacity is driven by an applied electrochemical potential rather than by O_2 or other chemical oxidants. Furthermore, it is noteworthy if the power to supply electrochemical potential comes directly from renewable energy such as solar light, the electrocatalytic oxidation of HMF would be a more promising approach. Fortunately, this idea was realized in 2005 by constructing a photoelectrochemical cell (PEC) (Cha and Choi, 2015). A nearly 100% FDCA yield and more than 93% faradaic efficiency were obtained. In this PEC system, an n-type nanoporous $BiVO_4$ electrode was used as a photoanode to generate photoexcited holes for the oxidation of 2,2,6,6-tetramethylpiperidine-1-oxyl (TEMPO) to $TEMPO^+$, which was further responsible for the oxidization of HMF to FDCA in 0.5 M borate buffer solution (pH 9.2). Meanwhile, the separated electrons were subsequently transferred to Pt cathode to reduce water to H_2. The high faradaic efficiency (FE) achieved for the FDCA formation indicated that the TEMPO oxidation is kinetically much more favorable than the water oxidation. Compared with electrochemical TEMPO-mediated HMF oxidation, the onset potential necessary to

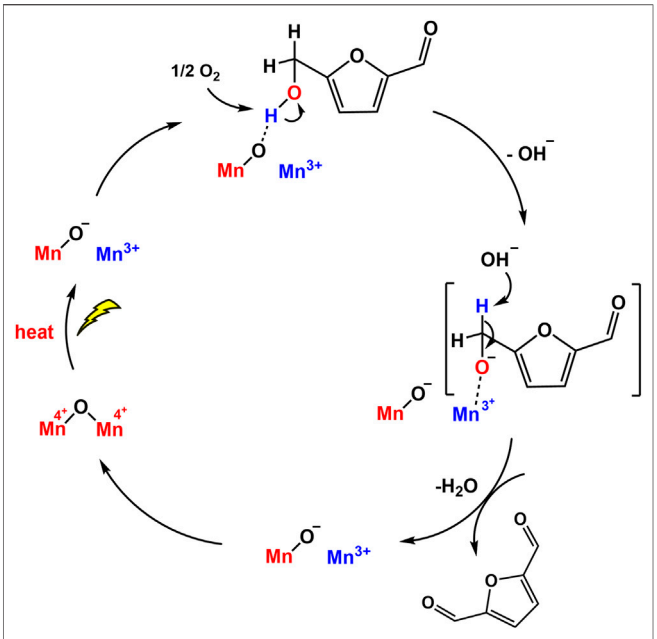

FIGURE 9 | Proposed mechanism for the photo-oxidation of HMF into DFF promoted by MnO_2 nanorods.

initiate photooxidation of TEMPO decreased considerably. This is because the photogenerated holes in $BiVO_4$ already have sufficient overpotential for TEMPO oxidation before an external bias is applied, significantly decreasing the external energy input for the PEC operation (**Figure 10**). The role of the applied bias is just to enhance the electron-hole pair separation to ensure that more photogenerated holes are available on the $BiVO_4$ electrode surface for HMF oxidation.

Photo-Reduction Reactions

It is interesting to find that most of studies focus on the oxidation of furan-based feedstocks, and few literatures have been reported in regard of photocatalytic reduction processes. In terms of thermodynamics and kinetics, the hydrogenation of C=C group is much more favorable than that of C=O double bond. Furthermore, the competitive adsorption of C=C and C=O groups at the catalyst surface also remains a challenge.

Guo et al. first reported that photocatalytic reduction of HMF into DHMF can be achieved by using a platinum catalyst supported on graphitic carbon nitride (Pt/g-C_3N_4) with trimethylamine as a sacrificial electron donor (Guo and Chen, 2016). The Pt/g-C_3N_4, as tandem catalyst, not only promoted the photo-induced water splitting to produce hydrogen but also facilitated the HMF reduction by activating the produced hydrogen. However, the catalytic performance of Pt/g-C_3N_4 was not ideal, and the yield of DHMF was low (6.5% yield with TOF of 0.457 h^{-1} at 80°C). Thus, there is substantial interest in designing a more effective photocatalyst for the reduction of HMF.

In the heterogeneous photocatalytic furan derivatives reduction reaction, there are two main photo-reduction mechanisms. The first is the direct hydrogen transfer from the hydrogen donor to the acceptor *via* a formation of a six-membered transition state. For example, Zhang and co-workers reported that mesoporous carbon supported metallic Cu and Cu_2O NPs have a synergistic effect on the selective hydrogenation of furfural (FAL) to furfuryl alcohol (FOL) under solar light irradiation with isopropanol as hydrogen source (Zhang and Li, 2019). Cu act as a bridge to promote the electron transfer from Cu_2O to carbon support due to the work function difference between Cu and Cu_2O, and the visible light irradiation facilitates this process. Meanwhile, the electron-rich mesoporous carbon favors the adsorption of C=O bond in the terminal of FAL. The separated photogenerated holes oxidize the isopropanol to yield acetone and protons, which then transfer to the mesoporous carbon adsorbed C=O bond to form FOL through a six-membered transition state (**Figure 11**). After 14 h reaction, 94.3% of FAL was consumed and a FOL yield of 90.9% was achieved.

Alternatively, the hydrogen from external hydrogen donor could be oxidized to form activated hydrogen species on catalyst surface, and then participate in the reduction reaction, namely indirect hydrogen transfer. Wang et al. reported that a Cu-H species can be formed on the surface of carbon-coated Cu NPs *in-situ* by activating H_2 with hot electrons generated by LSPR effect. The C=O group of FAL adsorbed on Cu is then attacked by two H atoms to produce FOL (**Figure 12**). Decreased yield of FOL was observed when adding a hydrogen abstracting agent 2,2′,6,6-

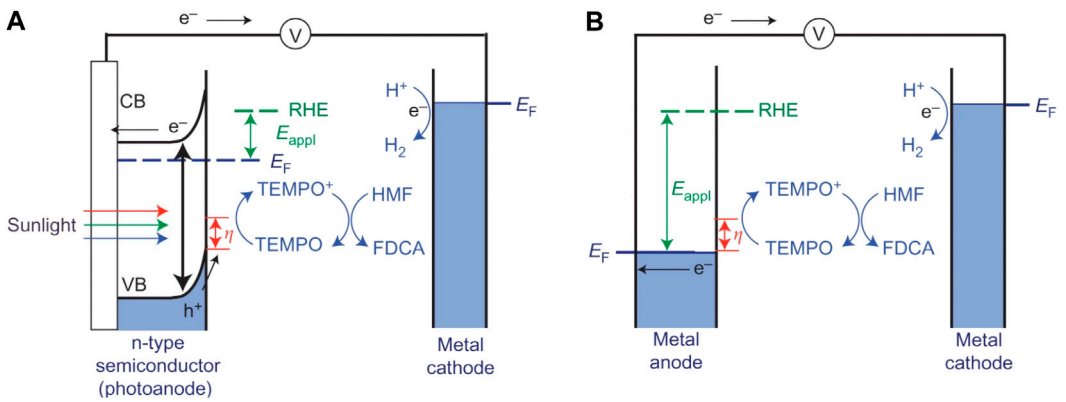

FIGURE 10 | Schematic comparison of **(A)** photoelectrochemical cells and **(B)** electrochemical cells for TEMPO-mediated HMF oxidation.

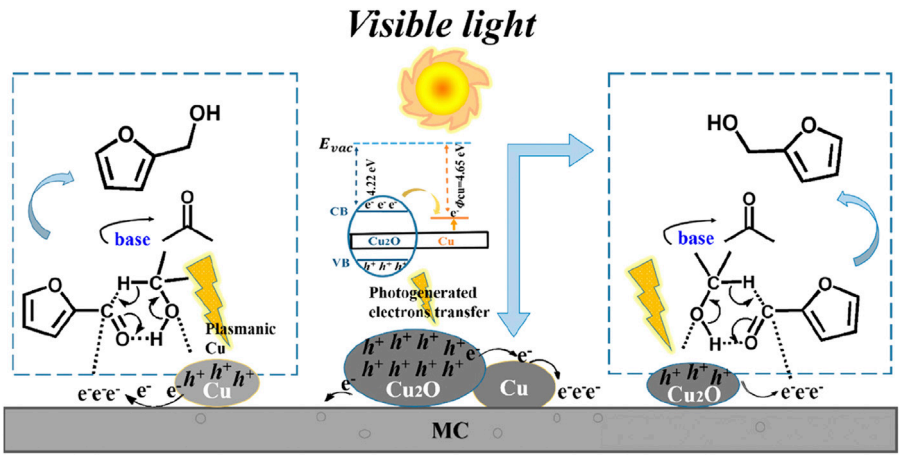

FIGURE 11 | Proposed mechanism of photocatalytic hydrogenation of furfural to produce furfuryl alcohol over MC supported Cu and Cu_2O catalyst.

tetramethylpiperidine N-oxyl (TEMPO), proving the formation of Cu-H species. Carbon-encapsulated Cu NPs were synthesized by pyrolysis of Cu-MOF ($[Cu_3(BTC)_2]$) in an H_2/Ar flow at 600°C. Higher pyrolysis temperature led to thicker carbon cladding, hindering light absorption, and a lower pyrolysis temperature of 400°C favored the generation of Cu (II) species, which showed weaker performance in the hydrogenation of FAL than the 600°C-formed metallic Cu. DFT results confirmed that the strong s-p-d hybridization facilitate the electron transfer between exposed Cu atoms and the C support and enhance the stability of Cu NPs (Wang et al., 2020).

A SiC-supported Au NPs (Au/SiC) exhibited high selectivity (>90%) for the photocatalytic hydrogenation of a series of α,β-unsaturated aldehydes such as HMF and FAL under visible light irradiation (Hao et al., 2016). The elaborate designed plasmonic metal/semiconductor structure forms a built-in electric field at the Au/SiC interface, which enhances the directional electron transfer. LSPR leads to the injection of hot electrons into the CB of SiC, resulting in the formation of positively charged Au NPs and electron-rich active sites at the interface of Au/SiC. The high electron density and steric hindrance effect at the Au/SiC interface are beneficial for the adsorption of terminal C=O groups rather than the bulky rings. Isopropanol can be oxidized on the positively charged Au surface to generate acetone and reactive hydrogen species. The latter is available for the reduction of aldehyde group to obtain FOL. A similar mechanism was also demonstrated in an $Au/CuCo_2O_4$ system (Hu et al., 2020), where a nearly 100% selectivity to DHMF and a 93% conversion to HMF were achieved within 1 h.

CONCLUSIONS AND PERSPECTIVES

Carbohydrate, including cellulose and hemicellulose, constitute more than 60% of lignocellulosic biomass and represent the most abundant source of renewable carbon in nature. Abundant and free solar light as the driving force, unique photogenerated reactive species (e.g., h^+, e^-, $^{\bullet}OH$, $^{\bullet}O_2^-$, and $^1O_2$) and mild reaction conditions make photocatalysis a "dream reaction". Using solar energy to selectively convert lignocellulosic biomass into value-added chemicals and fuels *via* photocatalysis at room temperature and pressure is an innovative but proven idea that could bring some merits from an energy and environmental perspective, such as reducing our carbon footprint and dependence on fossil fuels. Although the production of fine chemicals and biofuels is still small and far from satisfying the needs of society, it can be safely expected that biofuels will become the most important part of the global energy

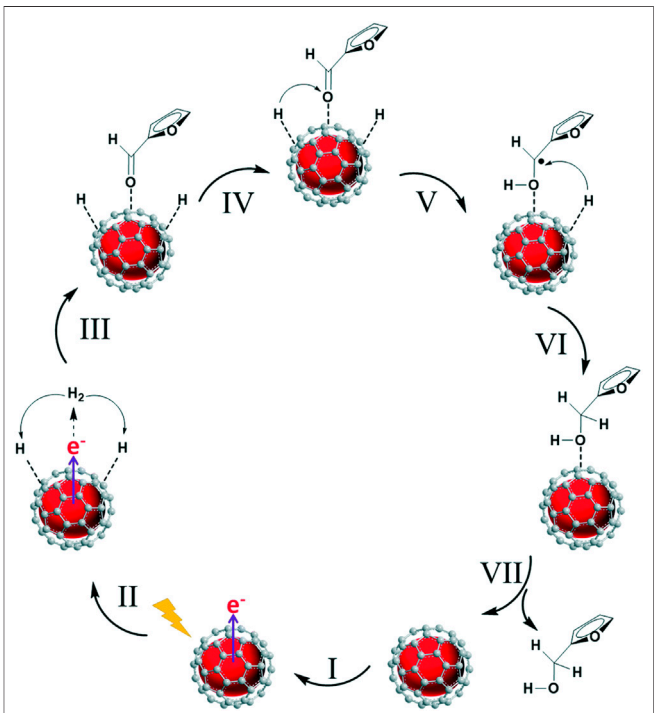

FIGURE 12 | Schematic representation of furfural hydrogenation to furfuryl alcohol on the Cu@C catalyst.

TABLE 1 | Photocatalytic conversion of cellulose in the literature.

Year	Substrate	Photocatalyst	Media	Atmosphere	Light source	Irradiation time (h)	Temperature (°C)	Product (selectivity, %)	Ref
2015	Cellulose	Au-HYT	Water, EMIMCl	NA	Visible light (0.5 W/cm^2)	16	140	Glucose (yield 48.1), HMF (yield 10.6)	Wang et al. (2015)
2018	Cellulose	Ir/HY_3	Water, EMIMCl	NA	Xenon lamp (300 W, 420–800 nm)	8	90	Cellobiose (10.9), Glucose (40.4), HMF (24)	Zhang et al. (2018a)
2018	Cellulose	P25-SO_4^{2-}-Ni_xS_y	Water	N_2	Xenon lamp (500 W)	3	80	H_2 (181.2 μmol)	Hao et al. (2018)
2018	Cellulose	TiO_2/NiO_x@C_g	Water	N_2	Xenon lamp (500 W)	5	80	H_2 (82.9 μmol h^{-1})	Zhang et al. (2018b)

TABLE 2 | Photocatalytic conversion of glucose in the literature.

Year	Substrate	Photocatalyst	Media	Light source	Irradiation time (min)	Conversion (%)	Products (selectivity, %)	Ref
2011	Glucose	TiO_2 powder	Water and acetonitrile (50: 50 v/v)	Mercury lamp (125 W)	10	11	Gluconic acid, glucaric acid, and arabitol (total 71.3)	Colmenares et al. (2011)
2017	Glucose	Nano-TiO_2	0.03 M NaOH aqueous	Mercury lamp (125 W)	9	~100	Formic acid (35)	Jin et al. (2017)
2017	Glucose	AuNPs/TiO_2 with 3 wt% Au	Water, Na_2CO_3	UV light (λ = 350–400 nm, 0.3 W cm^{-2})	4	99	Gluconic acid (yield 94)	Zhou et al. (2017)
2017	Glucose	AuNPs/TiO_2 with 3 wt% Au	Water, Na_2CO_3	Visible light irradiation (λ = 420–780 nm, 0.3 W cm^{-2})	4	99	Gluconic acid (yield 99)	Zhou et al. (2017)
2019	Glucose	H-ZSM-5/FePz $(SBu)_8$	Water and H_2O_2 (H_2O_2: Glucose = 3.3:1)	Xenon lamp (1.70 W cm^{-2}, λ > 420 nm)	4	35.8	Gluconic acid (31.9),Glucaric acid (13.1),Arabinose (17.3),Glycerol (1.7),Formic acid (13)	Chen et al. (2019)
2019	Glucose	SnO_2/FePz $(SBu)_8$	Water	Xenon lamp (2 W cm^{-2})	3	34.2	Gluconic acid (32.9),Glucaric acid (12.9),Formic acid (6.4)	Zhang et al. (2019)
2020	Glucose	TiO_2/HPW/CoPz	Water	Xenon lamp (1.70 W cm^{-2})	3	22.2	Gluconic acid (63.5),Glucaric acid (16.9)	Yin et al. (2020)
2020	Glucose	B/N-doped TiO_2	Water and acetonitrile (10: 90 v/v)	Mercury lamp (450 W, 250–365 nm)	3	93.1	Xylitol (yield 6),Gluconic acid (yield 6.5),Formic acid (yield 45),Arabinose (yield 30)	Suriyachai et al. (2020)
2020	Glucose	Ag/N-doped TiO_2	Water and acetonitrile (10: 90 v/v)	Mercury lamp (450 W, 250–365 nm)	3	97.7	Xylitol (yield 9),Gluconic acid (yield 2),Formic acid (yield 46),Arabinose (yield 30)	Suriyachai et al. (2020)

market in the foreseeable future. Despite tremendous efforts have been devoted in this field, photocatalytic transformation of biomass is still at an early stage and lags behind in terms of efficiency and cost. What is most surprising is that, to the best of our knowledge, few studies involving photocatalytic hemicellulose have been reported. There is still a long and tough way to go to achieve industrial applications.

(1) TiO_2 and g-C_3N_4 based materials are the most frequently used photocatalysts in biomass valorization because of their excellent performance in both oxidative and reductive reactions. But it is not difficult to find that the lack of innovation in catalyst design in recent years has presented a dilemma of old wine in new bottles. Thus, it is extremely important to design novel, effective and noble-metal-free photocatalysts to convert carbohydrates to valuable products with high conversion and selectivity under the guidance of pairing the band edge positions of semiconductors with redox levels of the targeted oxidation and reduction half reactions. Meanwhile, achieving one-pot reaction to avoid costly intermediate separation processes is also worth consideration.

(2) In the future, advanced characterization techniques such as SEM, TEM, XRD, XPS, FT-IR and DRIFT can be deliberately combined with quantum chemical calculations, i.e., density functional theory, to get an atomic-level insight into the structure-property relationships of photocatalysts, favorable reaction pathways and the interactions between reactants and catalysts (Lu et al., 2016; Liu et al., 2018). Moreover, the application of accurate detection technologies (i.e., *in situ*

TABLE 3 | Photocatalytic conversion of HMF and furfural in the literature.

Year	Substrate	Photocatalyst	Media	Atmosphere	Light source	Irradiation time (h)	Conversion (%)	Products (selectivity, %)	Ref
2013	HMF	TiO_2	Water	Air	Fluorescent lamps (λ = 365 nm, 3.0 mW/cm^2)	7	NA	DFF (22)	Yurdakal et al. (2013)
2015	HMF	$BiVO_4$ electrode	0.5 M borate buffer solution (pH = 9.2), TEMPO	NA	AM 1.5 G illumination (100 mW/cm^2)	NA	99.24	FDCA (99.6)	Cha and Choi (2015)
2016	HMF	Pt/g-C_3N_4	Triethylamine, water	NA	Xenon lamp (210 W, λ > 420 nm, 80°C)	4	NA	DHMF (yield 6.5)	Guo and Chen (2016)
2016	HMF	Au/SiC	KOH, isopropyl alcohol	Ar	Xenon lamp (λ = 400–800 nm, 1 W/cm^2)	4	90	DHMF (93)	Hao et al. (2016)
2017	HMF	g-C_3N_4	Water	Air	Fluorescent lamps (λ = 340–420 nm)	4	40	DFF (45)	Krivtsov et al. (2017a)
2017	HMF	g-C_3N_4	Acetonitrile + benzotrifluoride	O_2	Xenon lamp (300 W, λ > 360 nm)	6	85.6	DFF (47.2)	Wu et al. (2017)
2017	HMF	Ni/CdS	Water	N_2	Blue LED (λ = 450 nm, 8 W)	22	20	DFF (~100), H_2	Han et al. (2017)
2017	HMF	CoPz/g-C_3N_4	$Na_2B_4O_7$ buffer solution (pH = 9.18)	Air	Xenon lamp (λ = 300–1,000 nm, 0.5 W/cm^2)	14	99.1	FDCA (97)	Xu et al. (2017)
2018	HMF	PCN-H_2O_2	Water	NA	Natural sunlight	4	20	DFF (88)	Ilkaeva et al. (2018)
2019	HMF	SGCN	Water	NA	AM 1.5 G illumination (100 mW/cm^2)	6	15	DFF (>99),H_2 (12 μmol h^{-1}m^{-2})	Battula et al. (2019)
2019	HMF	MnO_2	Acetonitrile	Air	Homemade LED photo-reactor	6	99	DFF (~100)	Giannakoudakis et al. (2019)
2019	Furfural	Cu/Cu2O-MC	Isopropanol	N_2	White light LED (65 mW/cm^2)	14	94.3	Furfuryl alcohol (yield 90.9)	Zhang and Li (2019)
2020	HMF	NiS/$Zn_3In_2S_6$	Water	N_2	Xenon lamp (300 W, λ > 400 nm)	4	95	DFF (94.1),H_2 (120 μmol h^{-1}g^{-1})	Meng et al. (2020)
2020	HMF	Au/$CuCo_2O_4$	KOH, isopropanol	N_2	Xenon lamp (300 W, λ = 420–800 nm)	1	93	DHMF (100)	Hu et al. (2020)
2020	Furfural	Cu@C	Isopropanol	H_2	Visible light irradiation (0.5 W cm^{-2})	24	NA	Furfuryl alcohol (yield 99.4)	Wang et al. (2020)

NMR spectroscopy, electron paramagnetic resonance (EPR), transient absorption spectroscopy (TAS)) to trace generated intermediates and active surface-bound radicals will help to elucidate the reaction mechanism of biomass photocatalysis (Xia et al., 2020). Subsequent product separation, purification and identification should also be followed up (GC-MS, HPLC, GPC, 2D HSQC NMR).

(3) The engineering design and scale-up of the reactor for the conversion of biomass still need to be modified due to some foremost issues such as phase interaction between biomass and catalyst, heat and mass transfer. For traditional batch reactor, higher transparency for the irradiated light, lower light scattering and easy operation should be the basic requirements. On the other hand, due to the excellent control over photon and heat and mass transfer, designing microfluidic reactors holds great potential in improving the performance of photocatalytic system (Colmenares et al., 2017). Currently, studies supported by microfluidic reactors are still rare (Nguyen et al., 2014; Li et al., 2020), but the development of microfluidic reactors to improve the photocatalytic conversion of biomass is an important research direction in the near future.

(4) The selection of an appropriate reaction temperature range always plays an important role in product selectivity; generally speaking, too high a temperature will lead to the generation of undesired by-products, while too low a temperature will prolong the reaction time and greatly reduce the catalyst activity. Reaction time optimization is also extremely important since it determines the contact time between the reactants and the photocatalyst, which is likely to alter the product distribution.

(5) Solvent is essential for most organic synthesis and catalytic reactions. It plays the role of facilitating heat and mass

transfer and allow the reactant molecules to be homogeneously dispersed in the reaction medium. A good solvent for photocatalytic carbohydrates transformation should follow several requirements: 1) good solubility for carbohydrates and its derivatives; 2) be compatible with the chosen light source and reactor (solvent is neither a strong light absorber, nor does it corrode the reactor wall); 3) be physically and chemically stable under photocatalytic conditions; 4) nontoxic, low-cost, can be easily recycled and reused (Su et al., 2014). Water is the most abundant and environmental-friendly solvent, but receive less attention due to weaker dissolving ability than some organic solvents (ethanol, acetonitrile, trifluorotoluene) and the potential for the generation of nonselective hydroxyl radicals.

(6) The conversion and selectivity of photocatalytic biomass transformation are not yet as high as those of conventional thermocatalysis. If catalytic production of fuels and chemicals from biomass can be scale up from laboratory to large biorefineries, in-depth studies of mixing efficiency, reaction mechanisms, reaction thermodynamics and kinetics, heat and mass transport phenomena in large reactors are required (Su et al., 2014).

In this review, recent advances on the photocatalytic production of important organic acids and furan chemicals from carbohydrates and their derivatives have been well summarized. Although most of current transformation methods are theoretically and technically feasible, they are not economical. However, these contributive studies are now bringing us closer to a more promising future which is featured with biomass-based technologies.

AUTHOR CONTRIBUTIONS

HC, KW, FZ, ZZ, YZ, and DL discussed the topic together. HZ and HC drew the pictures. HC and YZ wrote the manuscript. All authors contributed to the article and approved the submitted version.

FUNDING

This work was financially supported by National Natural Science Foundation of China (No. 22008073), and Shanghai Sailing Program (No. 20YF1410600).

REFERENCES

Battula, V. R., Jaryal, A., and Kailasam, K. (2019). Visible light-driven simultaneous H2 production by water splitting coupled with selective oxidation of HMF to DFF catalyzed by porous carbon nitride. *J. Mater. Chem. A* 7, 5643–5649. doi:10.1039/c8ta10926e

Benkó, T., Beck, A., Frey, K., Srankó, D. F., Geszti, O., Sáfrán, G., et al. (2014). Bimetallic Ag-Au/SiO_2 catalysts: formation, structure and synergistic activity in glucose oxidation. *Appl. Catal. A Gen.* 479, 103–111. doi:10.1016/j.apcata.2014.04.027

Cha, H. G., and Choi, K. S. (2015). Combined biomass valorization and hydrogen production in a photoelectrochemical cell. *Nat. Chem.* 7, 328–333. doi:10.1038/nchem.2194

Chatterjee, C., Pong, F., and Sen, A. (2015). Chemical conversion pathways for carbohydrates. *Green Chem.* 17, 40–71. doi:10.1039/c4gc01062k

Chen, R., Yang, C., Zhang, Q., Zhang, B., and Deng, K. (2019). Visible-light-driven selective oxidation of glucose in water with H-ZSM-5 zeolite supported biomimetic photocatalyst. *J. Catal.* 374, 297–305. doi:10.1016/j.jcat.2019.04.044

Cheng, M., Zhang, Q., Yang, C., Zhang, B., and Deng, K. (2019). Photocatalytic oxidation of glucose in water to value-added chemicals by zinc oxide-supported cobalt thioporphyrazine. *Catal. Sci. Technol.* 9, 6909–6919. doi:10.1039/c9cy01756a

Climent, M. J., Corma, A., and Iborra, S. (2011). Converting carbohydrates to bulk chemicals and fine chemicals over heterogeneous catalysts. *Green Chem.* 13, 520–540. doi:10.1039/c0gc00639d

Colmenares, J. C., and Magdziarz, A. (2013). Room temperature versatile conversion of biomass-derived compounds by means of supported TiO_2 photocatalysts. *J. Mol. Catal. A Chem.* 366, 156–162. doi:10.1016/j.molcata.2012.09.018

Colmenares, J. C., Magdziarz, A., and Bielejewska, A. (2011). High-value chemicals obtained from selective photo-oxidation of glucose in the presence of nanostructured titanium photocatalysts. *Bioresour. Technol.* 102, 11254–11257. doi:10.1016/j.biortech.2011.09.101

Colmenares, J. C., Magdziarz, A., Chernyayeva, O., Lisovytskiy, D., Kurzydłowski, K., and Grzonka, J. (2013a). Sonication-Assisted low-temperature routes for the synthesis of supported Fe-TiO2Econanomaterials: partial photooxidation of glucose and phenol aqueous degradation. *ChemCatChem* 5, 2270–2277. doi:10.1002/cctc.201300025

Colmenares, J. C., Magdziarz, A., Kurzydlowski, K., Grzonka, J., Chernyayeva, O., and Lisovytskiy, D. (2013b). Low-temperature ultrasound-promoted synthesis of Cr-TiO_2-supported photocatalysts for valorization of glucose and phenol degradation from liquid phase. *Appl. Catal. B Environ.* 134–135, 136–144. doi:10.1016/j.apcatb.2013.01.020

Colmenares, J. C., Varma, R. S., and Nair, V. (2017). Selective photocatalysis of lignin-inspired chemicals by integrating hybrid nanocatalysis in microfluidic reactors. *Chem. Soc. Rev.* 46, 6675–6686. doi:10.1039/c7cs00257b

Credou, J., and Berthelot, T. (2014). Cellulose: from biocompatible to bioactive material. *J. Mater. Chem. B* 2, 4767–4788. doi:10.1039/c4tb00431k

Da Vià, L., Recchi, C., Gonzalez-Yañez, E. O., Davies, T. E., and Lopez-Sanchez, J. A. (2017). Visible light selective photocatalytic conversion of glucose by TiO2. *Appl. Catal. B Environ.* 202, 281–288. doi:10.1016/j.apcatb.2016.08.035

De, S., Saha, B., and Luque, R. (2015). Hydrodeoxygenation processes: advances on catalytic transformations of biomass-derived platform chemicals into hydrocarbon fuels. *Bioresour. Technol.* 178, 108–118. doi:10.1016/j.biortech.2014.09.065

Deng, W., Zhang, Q., and Wang, Y. (2014). Catalytic transformations of cellulose and cellulose-derived carbohydrates into organic acids. *Catal. Today* 234, 31–41. doi:10.1016/j.cattod.2013.12.041

DiMeglio, J. L., Breuhaus-Alvarez, A. G., Li, S., and Bartlett, B. M. (2019). Nitrate-mediated alcohol oxidation on cadmium sulfide photocatalysts. *ACS Catal.* 9, 5732–5741. doi:10.1021/acscatal.9b01051

Fan, H., Li, G., Yang, F., Yang, L., and Zhang, S. (2011). Photodegradation of cellulose under UV light catalysed by TiO2. *J. Chem. Technol. Biotechnol.* 86, 1107–1112. doi:10.1002/jctb.2632

Giannakoudakis, D. A., Nair, V., Khan, A., Deliyanni, E. A., Colmenares, J. C., and Triantafyllidis, K. S. (2019). Additive-free photo-assisted selective partial oxidation at ambient conditions of 5-hydroxymethylfurfural by manganese (IV) oxide nanorods. *Appl. Catal. B Environ.* 256. doi:10.1016/j.apcatb.2019.117803

Guerriero, A., Bricout, H., Sordakis, K., Peruzzini, M., Monflier, E., Hapiot, F., et al. (2014). Hydrogen production by selective dehydrogenation of HCOOH catalyzed by Ru-biaryl sulfonated phosphines in aqueous solution. *ACS Catal.* 4, 3002–3012. doi:10.1021/cs500655x

Guo, Y., and Chen, J. (2016). Photo-induced reduction of biomass-derived 5-hydroxymethylfurfural using graphitic carbon nitride supported metal catalysts. *RSC Adv.* 6, 101968–101973. doi:10.1039/c6ra19153c

Han, G., Jin, Y. H., Burgess, R. A., Dickenson, N. E., Cao, X. M., and Sun, Y. (2017). Visible-light-driven valorization of biomass intermediates integrated with H2 production catalyzed by ultrathin Ni/CdS nanosheets. *J. Am. Chem. Soc.* 139, 15584–15587. doi:10.1021/jacs.7b08657

Hao, C. H., Guo, X. N., Pan, Y. T., Chen, S., Jiao, Z. F., Yang, H., et al. (2016). Visible-light-driven selective photocatalytic hydrogenation of cinnamaldehyde over Au/SiC catalysts. *J. Am. Chem. Soc.* 138, 9361–9364. doi:10.1021/jacs.6b04175

Hao, H., Zhang, L., Wang, W., and Zeng, S. (2018). Facile modification of titania with nickel sulfide and sulfate species for the photoreformation of cellulose into hydrogen. *ChemSusChem* 11, 2810–2817. doi:10.1002/cssc.201800743

Haynes, T., Dubois, V., and Hermans, S. (2017). Particle size effect in glucose oxidation with Pd/CB catalysts. *Appl. Catal. Gen.* 542, 47–54. doi:10.1016/j.apcata.2017.05.008

Hu, L., Lin, L., Wu, Z., Zhou, S., and Liu, S. (2015). Chemocatalytic hydrolysis of cellulose into glucose over solid acid catalysts. *Appl. Catal. B Environ.* 174–175, 225–243. doi:10.1016/j.apcatb.2015.03.003

Hu, L., Lin, L., Wu, Z., Zhou, S., and Liu, S. (2017). Recent advances in catalytic transformation of biomass-derived 5-hydroxymethylfurfural into the innovative fuels and chemicals. *Renew. Sustain. Energy Rev.* 74, 230–257. doi:10.1016/j.rser.2017.02.042

Hu, L., Xu, J., Zhou, S., He, A., Tang, X., Lin, L., et al. (2018). Catalytic advances in the production and application of biomass-derived 2,5-dihydroxymethylfuran. *ACS Catal.* 8, 2959–2980. doi:10.1021/acscatal.7b03530

Hu, G., Huang, Z.-P., Hu, C.-X., Zhang, Z.-Q., Liu, R.-T., Li, X.-Y., et al. (2020). Selective photocatalytic hydrogenation of α,β-unsaturated aldehydes on Au/CuCo2O4 nanotubes under visible-light irradiation. *ACS Sustain. Chem. Eng.* 8, 8288–8294. doi:10.1021/acssuschemeng.0c01852

Huang, Y.-B., and Fu, Y. (2013). Hydrolysis of cellulose to glucose by solid acid catalysts. *Green Chem.* 15, 1095–1111. doi:10.1039/c3gc40136g

Ilkaeva, M., Krivtsov, I., García-López, E. I., Marcì, G., Khainakova, O., García, J. R., et al. (2018). Selective photocatalytic oxidation of 5-hydroxymethylfurfural to 2,5-furandicarboxaldehyde by polymeric carbon nitride-hydrogen peroxide adduct. *J. Catal.* 359, 212–222. doi:10.1016/j.jcat.2018.01.012

Jin, B., Yao, G., Wang, X., Ding, K., and Jin, F. (2017). Photocatalytic oxidation of glucose into formate on nano TiO2 catalyst. *ACS Sustain. Chem. Eng.* 5, 6377–6381. doi:10.1021/acssuschemeng.7b00364

Kiely, D. E., Chen, L., and Lin, T. H. (1994). Hydroxylated nylons based on unprotected esterified D-glucaric acid by simple condensation reactions. *J. Am. Chem. Soc.* 116, 571–578. doi:10.1021/ja00081a018

Kim, G., Lee, S.-H., and Choi, W. (2015). Glucose-TiO 2 charge transfer complex-mediated photocatalysis under visible light. *Appl. Catal. B Environ.* 162, 463–469. doi:10.1016/j.apcatb.2014.07.027

Klemm, D., Heublein, B., Fink, H. P., and Bohn, A. (2005). Cellulose: fascinating biopolymer and sustainable raw material. *Angew Chem. Int. Ed. Engl.* 44, 3358–3393. doi:10.1002/anie.200460587

Krivtsov, I., García-López, E. I., Marcì, G., Palmisano, L., Amghouz, Z., García, J. R., et al. (2017a). Selective photocatalytic oxidation of 5-hydroxymethyl-2-furfural to 2,5-furandicarboxyaldehyde in aqueous suspension of g-C_3N_4. *Appl. Catal. B Environ.* 204, 430–439. doi:10.1016/j.apcatb.2016.11.049

Krivtsov, I., Ilkaeva, M., Salas-Colera, E., Amghouz, Z., García, J. R., Díaz, E., et al. (2017b). Consequences of nitrogen doping and oxygen enrichment on titanium local order and photocatalytic performance of TiO2 anatase. *J. Phys. Chem. C* 121, 6770–6780. doi:10.1021/acs.jpcc.7b00354

Li, C., Zhao, X., Wang, A., Huber, G. W., and Zhang, T. (2015). Catalytic transformation of lignin for the production of chemicals and fuels. *Chem. Rev.* 115, 11559–11624. doi:10.1021/acs.chemrev.5b00155

Li, J., Yin, J., Yang, C., Xu, S., Zhou, Q., Zhang, B., et al. (2018). Photocatalyst with annulated binuclear thioporphyrazine-enhancing photocatalytic performance by expansion of a π-electron system. *Catal. Sci. Technol.* 8, 5616–5622. doi:10.1039/c8cy01626g

Li, S., Hao, Z., Wang, K., Tong, M., Yang, Y., Jiang, H., et al. (2020). Visible light-enabled selective depolymerization of oxidized lignin by an organic photocatalyst. *Chem. Commun.* 56, 11243–11246. doi:10.1039/D0CC01127D

Liu, C., Zhang, J., Huang, J., Zhang, C., Hong, F., Zhou, Y., et al. (2017). Efficient aerobic oxidation of glucose to gluconic acid over activated carbon-supported gold clusters. *ChemSusChem* 10, 1976–1980. doi:10.1002/cssc.201700407

Liu, H., Li, H., Lu, J., Zeng, S., Wang, M., Luo, N., et al. (2018). Photocatalytic cleavage of C-C bond in lignin models under visible light on mesoporous graphitic carbon nitride through π-π stacking interaction. *ACS Catal.* 8, 4761–4771. doi:10.1021/acscatal.8b00022

Liu, X., Duan, X., Wei, W., Wang, S., and Ni, B.-J. (2019). Photocatalytic conversion of lignocellulosic biomass to valuable products. *Green Chem.* 21, 4266–4289. doi:10.1039/c9gc01728c

Lu, J., Wang, M., Zhang, X., Heyden, A., and Wang, F. (2016). β-O-4 bond cleavage mechanism for lignin model compounds over Pd catalysts identified by combination of first-principles calculations and experiments. *ACS Catal.* 6, 5589–5598. doi:10.1021/acscatal.6b00502

Meng, S., Wu, H., Cui, Y., Zheng, X., Wang, H., Chen, S., et al. (2020). One-step synthesis of 2D/2D-3D NiS/Zn3In2S6 hierarchical structure toward solar-to-chemical energy transformation of biomass-relevant alcohols. *Appl. Catal. B Environ.* 266, 118617. doi:10.1016/j.apcatb.2020.118617

Nguyen, J. D., Matsuura, B. S., and Stephenson, C. R. (2014). A photochemical strategy for lignin degradation at room temperature. *J. Am. Chem. Soc.* 136, 1218–1221. doi:10.1021/ja4113462

Puga, A. V. (2016). Photocatalytic production of hydrogen from biomass-derived feedstocks. *Coord. Chem. Rev.* 315, 1–66. doi:10.1016/j.ccr.2015.12.009

Shaghaleh, H., Xu, X., and Wang, S. (2018). Current progress in production of biopolymeric materials based on cellulose, cellulose nanofibers, and cellulose derivatives. *RSC Adv.* 8, 825–842. doi:10.1039/c7ra11157f

Sheldon, R. A. (2014). Green and sustainable manufacture of chemicals from biomass: state of the art. *Green Chem.* 16, 950–963. doi:10.1039/c3gc41935e

Su, Y., Straathof, N. J., Hessel, V., and Noël, T. (2014). Photochemical transformations accelerated in continuous-flow reactors: basic concepts and applications. *Chemistry* 20, 10562–10589. doi:10.1002/chem.201400283

Suriyachai, N., Chuangchote, S., Laosiripojana, N., Champreda, V., and Sagawa, T. (2020). Synergistic effects of Co-doping on photocatalytic activity of titanium dioxide on glucose conversion to value-added chemicals. *ACS Omega* 5, 20373–20381. doi:10.1021/acsomega.0c02334

van Putten, R. J., Van Der Waal, J. C., De Jong, E., Rasrendra, C. B., Heeres, H. J., and De Vries, J. G. (2013). Hydroxymethylfurfural, a versatile platform chemical made from renewable resources. *Chem. Rev.* 113, 1499–1597. doi:10.1021/cr300182k

Wang, M., and Wang, F. (2019). Catalytic scissoring of lignin into aryl monomers. *Adv. Mater.* 31, 1901866. doi:10.1002/adma.201901866

Wang, L., Zhang, Z., Zhang, L., Xue, S., Doherty, W. O. S., O'hara, I. M., et al. (2015). Sustainable conversion of cellulosic biomass to chemicals under visible-light irradiation. *RSC Adv.* 5, 85242–85247. doi:10.1039/c5ra16616k

Wang, S., Dai, G., Yang, H., and Luo, Z. (2017). Lignocellulosic biomass pyrolysis mechanism: a state-of-the-art review. *Prog. Energy Combust. Sci.* 62, 33–86. doi:10.1016/j.pecs.2017.05.004

Wang, R., Liu, H., Wang, X., Li, X., Gu, X., and Zheng, Z. (2020). Plasmon-enhanced furfural hydrogenation catalyzed by stable carbon-coated copper nanoparticles driven from metal-organic frameworks. *Catal. Sci. Technol.* 10, 6483–6494. doi:10.1039/d0cy01162b

Wu, Q., He, Y., Zhang, H., Feng, Z., Wu, Y., and Wu, T. (2017). Photocatalytic selective oxidation of biomass-derived 5-hydroxymethylfurfural to 2,5-diformylfuran on metal-free g-C_3 N_4 under visible light irradiation. *Molecular Catalysis* 436, 10–18. doi:10.1016/j.mcat.2017.04.012

Wu, X., Luo, N., Xie, S., Zhang, H., Zhang, Q., Wang, F., et al. (2020). Photocatalytic transformations of lignocellulosic biomass into chemicals. *Chem. Soc. Rev.* 49, 6198–6223. doi:10.1039/D0CS00314J

Xia, B., Zhang, Y., Shi, B., Ran, J., Davey, K., and Qiao, S. Z. (2020). Photocatalysts for hydrogen evolution coupled with production of Valueâ€Added chemicals. *Small Methods* 4. doi:10.1002/smtd.202000063

Xu, S., Zhou, P., Zhang, Z., Yang, C., Zhang, B., Deng, K., et al. (2017). Selective oxidation of 5-hydroxymethylfurfural to 2,5-furandicarboxylic acid using O_2 and a photocatalyst of Co-thioporphyrazine bonded to g-C_3N_4. *J. Am. Chem. Soc.* 139, 14775–14782. doi:10.1021/jacs.7b08861

Yin, J., Zhang, Q., Yang, C., Zhang, B., and Deng, K. (2020). Highly selective oxidation of glucose to gluconic acid and glucaric acid in water catalyzed by an efficient synergistic photocatalytic system. *Catal. Sci. Technol.* 10, 2231–2241. doi:10.1039/c9cy02393c

Yurdakal, S., Tek, B. S., Alagöz, O., Augugliaro, V., Loddo, V., Palmisano, G., et al. (2013). Photocatalytic selective oxidation of 5-(Hydroxymethyl)-2-furaldehyde to 2,5-furandicarbaldehyde in water by using anatase, rutile, and brookite TiO_2 nanoparticles. *ACS Sustain. Chem. Eng.* 1, 456–461. doi:10.1021/sc300142a

Zakrzewska, M. E., Bogel-Łukasik, E., and Bogel-Łukasik, R. (2011). Ionic liquid-mediated formation of 5-hydroxymethylfurfural-a promising biomass-derived building block. *Chem. Rev.* 111, 397–417. doi:10.1021/cr100171a

Zhang, B., Li, J., Guo, L., Chen, Z., and Li, C. (2018a). Photothermally promoted cleavage of β-1,4-glycosidic bonds of cellulosic biomass on Ir/HY catalyst under mild conditions. *Appl. Catal. B Environ.* 237, 660–664. doi:10.1016/j.apcatb.2018.06.041

Zhang, L., Wang, W., Zeng, S., Su, Y., and Hao, H. (2018b). Enhanced H_2 evolution from photocatalytic cellulose conversion based on graphitic carbon layers on TiO_2/NiO_x. *Green Chem.* 20, 3008–3013. doi:10.1039/c8gc01398e

Zhang, C., and Wang, F. (2020). Catalytic lignin depolymerization to aromatic chemicals. *Acc. Chem. Res.* 53, 470–484. doi:10.1021/acs.accounts.9b00573

Zhang, H., Wu, Q., Guo, C., Wu, Y., and Wu, T. (2017a). Photocatalytic selective oxidation of 5-hydroxymethylfurfural to 2,5-diformylfuran over Nb_2O_5 under visible light. *ACS Sustain. Chem. Eng.* 5, 3517–3523. doi:10.1021/acssuschemeng.7b00231

Zhang, Z., Song, J., and Han, B. (2017b). Catalytic transformation of lignocellulose into chemicals and fuel products in ionic liquids. *Chem. Rev.* 117, 6834–6880. doi:10.1021/acs.chemrev.6b00457

Zhang, J. (2018). Conversion of lignin models by photoredox catalysis. *ChemSusChem* 11, 3071–3080. doi:10.1002/cssc.201801370

Zhang, M., and Li, Z. (2019). Cu/Cu_2O-MC (MC = mesoporous carbon) for highly efficient hydrogenation of furfural to furfuryl alcohol under visible light. *ACS Sustain. Chem. Eng.* 7, 11485–11492. doi:10.1021/acssuschemeng.9b01305

Zhang, Q., Ge, Y., Yang, C., Zhang, B., and Deng, K. (2019). Enhanced photocatalytic performance for oxidation of glucose to value-added organic acids in water using iron thioporphyrazine modified SnO_2. *Green Chem.* 21, 5019–5029. doi:10.1039/c9gc01647c

Zhang, Z., and Deng, K. (2015). Recent advances in the catalytic synthesis of 2,5-furandicarboxylic acid and its derivatives. *ACS Catal.* 5, 6529–6544. doi:10.1021/acscatal.5b01491

Zhou, B., Song, J., Zhang, Z., Jiang, Z., Zhang, P., and Han, B. (2017). Highly selective photocatalytic oxidation of biomass-derived chemicals to carboxyl compounds over Au/TiO_2. *Green Chem.* 19, 1075–1081. doi:10.1039/c6gc03022j

Zhou, Q., Xu, S., Yang, C., Zhang, B., Li, Z., and Deng, K. (2016). Modulation of peripheral substituents of cobalt thioporphyrazines and their photocatalytic activity. *Appl. Catal. B Environ.* 192, 108–115. doi:10.1016/j.apcatb.2016.03.059

Conflict of Interest: The authors declare that the research was conducted in the absence of any commercial or financial relationships that could be construed as a potential conflict of interest.